RESEARCH ARTICLE

NANO · MICRO small
www.small-journal.com

A Difluoro-Methoxylated Ending-Group Asymmetric Small Molecule Acceptor Lead Efficient Binary Organic Photovoltaic Blend

Weiwei Wu, Bosen Zou, Ruijie Ma, Jia Yao, Chunliang Li, Zhenghui Luo,* Bomin Xie, Memoona Qammar, Top Archie Dela Peña, Mingjie Li, Jiaying Wu, Chuluo Yang, Qunping Fan, Wei Ma, Gang Li, and He Yan**

Developing a new end group for synthesizing asymmetric small molecule acceptors (SMAs) is crucial for achieving high-performance organic photovoltaics (OPVs). Herein, an asymmetric small molecule acceptor, BTP-BO-4FO, featuring a new difluoro-methoxylated end-group is reported. Compared to its symmetric counterpart L8-BO, BTP-BO-4FO exhibits an upshifted energy level, larger dipole moment, and more sequential crystallinity. By adopting two representative and widely available solvent additives (1-chloronaphthalene (CN) and 1,8-diiodooctane (DIO)), the device based on PM6:BTP-BO-4FO (CN) photovoltaic blend demonstrates a power conversion efficiency (PCE) of 18.62% with an excellent open-circuit voltage (V_{OC}) of 0.933 V, which surpasses the optimal result of L8-BO. The PCE of 18.62% realizes the best efficiencies for binary OPVs based on SMAs with asymmetric end groups. A series of investigations reveal that optimized PM6:BTP-BO-4FO film demonstrates similar molecular packing motif and fibrillar phase distribution as PM6:L8-BO (DIO) does, resulting in comparable recombination dynamics, thus, similar fill factor. Besides, it is found PM6:BTP-BO-4FO possesses more efficient charge generation, which yields better V_{OC}–J_{SC} balance. This study provides a new ending group that enables a cutting-edge efficiency in asymmetric SMA-based OPVs, enriching the material library and shed light on further design ideas.

1. Introduction

Organic photovoltaics (OPVs) have recently entered a golden era, with power conversion efficiencies (PCEs) exceeding 19% in single-junction devices and surpassing 20% in tandem structures, but there is still a gap compared to other commercialized PVs.[1–15] To further enhance the efficiency of OPVs, it is crucial to achieve orderly molecular stacking, appropriate nanoscale phase separation, and a continuous donor/acceptor (D/A) network.[16–18] Fundamentally, the molecular crystallization, aggregation propensity in the film states, and donor–acceptor miscibility significantly impact active layer morphology formation. Consequently, optimizing the interaction within the photovoltaic layer is essential for achieving the desired morphology.

According to the concept of "like dissolves like", a molecular design approach to regulating molecular interaction involves precise control of polymer material polarity,

W. Wu, B. Zou, J. Yao, C. Li, T. A. Dela Peña, H. Yan
Department of Chemistry Department of Chemistry and Hong Kong Branch of Chinese National Engineering Research Center for Tissue Restoration and Reconstruction
The Hong Kong University of Science and Technology
Clear Water Bay, Hong Kong 999077, P. R. China
E-mail: hyan@ust.hk

R. Ma, G. Li
Department of Electrical and Electronic Engineering
Research Institute for Smart Energy (RISE)
Photonic Research Institute (PRI)
The Hong Kong Polytechnic University
Hong Kong 999077, P. R. China
E-mail: ruijie.ma@polyu.edu.hk

Z. Luo, C. Yang
Guangdong Provincial Key Laboratory of New Energy Materials Service Safety
Shenzhen Key Laboratory of New Information Display and Storage Materials
College of Materials Science and Engineering
Shenzhen University
Shenzhen 518060, P. R. China
E-mail: zhhuiluo@szu.edu.cn

The ORCID identification number(s) for the author(s) of this article can be found under https://doi.org/10.1002/smll.202402793

DOI: 10.1002/smll.202402793

given the substantial dependence of molecular interactions on polarity.[19] Essentially, molecular polarity is intricately linked to the characteristics of substituent groups and molecular structure.[20–23] Notably, end-group engineering is a prevalent and effective strategy. Incorporating electron-withdrawing substituents (fluorine, chlorine) and electron-donating substituents (methyl, methoxyl) into terminal groups can efficiently adjust optical absorption, energy levels, crystallinity, and varying molecular polarities. Moreover, asymmetric design can be a practical method for further efficiency enhancement.[24–32] Combining asymmetric strategies with end-group engineering could fine-tune molecular orientation, and stacking pattern reasonably, thus the asymmetric molecules typically exhibit stronger intermolecular interactions.

For instance, Chen and coworkers synthesized an asymmetric acceptor named BO-5Cl,[33] it can lead to OPVs that combine low non-radiative voltage losses and high charge generation efficiency. Incorporating BO-5Cl as the third component into PM6:BO-4Cl system achieves a high certified PCE of 18.2%. Cui et al proposed that the asymmetric structure contributes to more efficient electron-hole separation and stronger intermolecular π–π interaction followed by improving self-assembly behavior. The device based on their designed asymmetric acceptor BTP-Cl exhibited a very low ΔE_3 of 0.21 eV with a high PCE over 17% when paired with donor PM6.[34]Our team previously also developed an asymmetric SMA with fluoro-methoxylated terminal group, namely BTP-BO-3FO.[35] The asymmetric BTP-BO-3FO achieves a commendable efficiency of up to 15.80%, significantly surpassing the 10.2% efficiency of its symmetric counterpart, BTP-BO-SFO. Despite a high V_{OC} of 0.952 V obtained with the BTP-BO-3FO-based device, its inadequate charge separation caused by large bandgap and suboptimal active layer morphology results in relatively low short circuit current density (J_{SC}) and fill factor (FF). Consequently, its overall efficiency falls short compared to its other symmetric counterpart of L8-BO.

Based on the above consideration, to minimize the offset in energy levels while ensuring adequate charge separation, we introduced a fluorine atom into the fluorine- and methoxy-co-substituted terminal group to synthesize an IC-2FOMe terminal group and synthesized the corresponding asymmetric SMA, namely BTP-BO-4FO. First, the addition of a fluorine atom fine-tunes the molecular polarity, and strengthens electron-withdrawing ability, thereby enhancing the intramolecular charge transfer effect and broadening the absorption spectrum. Second, the introduction of fluorine atoms is helpful for forming non-covalent intermolecular interactions (F–S, F–H, F–F, etc.), which is beneficial for increasing the electron mobility of acceptor molecules and regulating the bulk morphology in blend system. By pairing with the polymer donor PM6 without additives, it realizes a decent efficiency as high as 17.33%, nearly the 17.36% efficiency of L8-BO. In addition to designing new materials, additive engineering also plays an important role in regulating morphology to achieve high PCEs. We utilized two common additives, 1-chloronaphthalene (CN) and 1,8-diodooctane (DIO), to finely adjust the active layer's morphology. As a result, CN treatment led to smaller pure domains and improved molecular stacking order, resulting in outstanding miscibility of the blend film and an impressive efficiency of 18.62% with an excellent V_{OC} of 0.933 V. It is the highest PCEs for binary OPVs based on SMAs with asymmetric terminal groups so far. This work underscores the advantage of incorporating two distinct terminal groups into SMAs to strike a balance between V_{OC} and J_{SC}, ultimately leading to enhanced PCE.

2. Results and Discussion

The chemical structures of the electron acceptor L8-BO, and derived asymmetric acceptors substituted with different end groups, BTP-BO-3FO and BTP-BO-4FO are depicted in **Figure 1a**. Figure S1 (Supporting Information) presents the detailed synthetic routes to IC-2FOMe and asymmetric SMA, BTP-BO-4FO, through a sequence of mature reactions reported previously. The synthesis procedures and characterization data, including NMR and mass spectra, are provided in Figures S1–S6 (Supporting Information). BTP-BO-4FO exhibits favorable solubility in common solvents, such as toluene, chlorobenzene (CB), chloroform (CF), and dichloromethane (DCM).

A notable advantage of Y-series molecules lies in their structured molecular arrangement and energetic states, both of which can impact absorption profiles significantly. The absorption spectra of the two acceptors were measured and compared in chloroform (CF) solutions as well as thin films. (Figure 1b; Figure S7, Supporting Information). In chloroform solutions, L8-BO and BTP-BO-4FO demonstrate closely aligned absorption profiles, with comparable maximum peaks at 732 and 729 nm, respectively. Upon transitioning to thin films, both BTP-BO-4FO and L8-BO exhibit a redshift in their maximum peaks by 70 nm. Notably, the BTP-BO-4FO film exhibits a sharper absorption edge compared to the L8-BO film, indicating a greater degree of ordered molecular packing in the solid state. Cyclic voltammetry was carried out to investigate the energy alignment of the thin films and the related results are displayed in Figure 1d and Figure S8 (Supporting Information). The lowest unoccupied molecular orbital (LUMO) and HOMO levels were determined to be −3.90 and −5.68 eV for L8-BO, and −3.83 and −5.65 eV for BTP-BO-4FO. Both the LUMO and HOMO levels of BTP-BO-4FO exhibit a slight upshift in comparison to those of L8-BO. The trend in energy level variations is corroborated through density functional theory (DFT) calculations based on the wb97xd/6–31 + g(d,p) level(Figure S9, Supporting Information).[36–38] Furthermore, conducting a detailed analysis of molecular interactions

B. Xie, Q. Fan, W. Ma
State Key Laboratory for Mechanical Behavior of Materials
Xi'an Jiaotong University
Xi'an 710049, P. R. China
M. Qammar
Department of Chemistry
The Hong Kong University of Science and Technology (HKUST)
Clear Water Bay Rd, Kowloon, Hong Kong 999077, P. R. China
T. A. Dela Peña, M. Li
Department of Applied Physics
The Hong Kong Polytechnic University
Hong Kong 999077, P. R. China
T. A. Dela Peña, J. Wu
Function Hub
Advanced Materials Thrust
The Hong Kong University of Science and Technology
Nansha, Guangzhou 511400, P. R. China

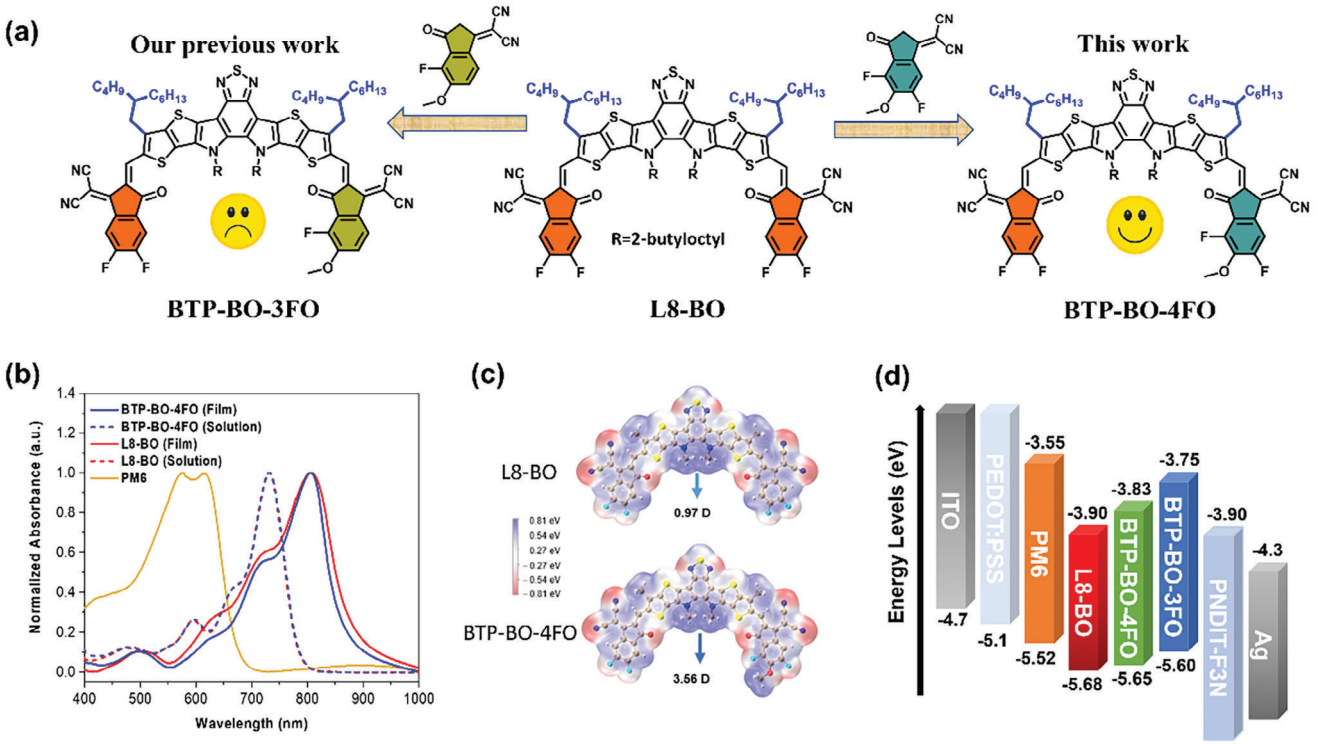

Figure 1. a) Chemical structures of BTP-BO-3FO, L8-BO, and BTP-BO-4FO. b) UV–vis absorption profiles of neat materials in CHCl3 solutions and films. c) Electrostatic potential of L8-BO and BTP-BO-4FO. d) Energy level distribution of PM6, L8-BO, BTP-BO-3FO, and BTP-BO-4FO.

and the electrostatic potential (ESP) distribution on the molecular surface is advantageous for understanding the compatibility between donors and acceptors. Significantly distinct ESP distributions between two molecules typically signify substantial intermolecular interactions, while similar ESP distributions suggest high compatibility (weak intermolecular interactions). In Figure 1c, the ESP distributions of two acceptors are displayed, where blue signifies positive potential and red indicates negative potential. Focusing on the end groups of BTP-BO-4FO, the introduction of methoxy groups resulted in a decrease in the ESP of the benzene due to the electron-donating nature of the methoxy groups (from 0.453 to 0.428 eV in Figure S10, Supporting Information), consequently displaying a higher dipole moment of 3.56D compared to L8-BO (0.97D) (Figure 1c). The significant difference in dipole moment at the terminals for asymmetric molecules may contribute to stronger intermolecular interactions, thereby enhancing the self-assembly behavior of the molecules.

Grazing-incidence wide-angle X-ray scattering (GIWAXS) measurements were conducted on the pristine films of BTP-BO-4FO and L8-BO to assess their crystal order and molecular stacking.[39–42] The results, as illustrated in **Figure 2**, strong signal peaks at q_r ≈0.430 Å^{-1} (d ≈14.6 Å) in the in-plane (IP) direction and at q_z ≈1.82 Å^{-1} (d ≈3.45 Å) in the out-of-plane (OOP) direction are observed in the neat L8-BO and BTP-BO-4FO films, signifying a predominant face-on molecular stacking orientation in both cases. Detailed parameters of peak intensity profiles along with IP/OOP direction are summarized in Tables S1 (Supporting Information). The peak intensity and CCL (21.7 Å) for π–π stacking along the out-of-plane (OOP) direction of pure BTP-BO-4FO film are larger than that of pure L8-BO (18.6 Å) film, suggesting a more ordered π–π stacking in BTP-BO-4FO film, which is beneficial to the charge transport in acceptor phase. It may be ascribed to its large dipole moment for enhanced intermolecular interaction. Moreover, BTP-BO-4FO displays multiple scattering peaks in both IP and OOP directions compared to the single peak observed in L8-BO, indicating that the asymmetric terminal group induces alterations in molecular lamellar packing order and π–π stacking order due to the disrupted structural symmetry.

To evaluate the photovoltaic performance of BTP-BO-4FO and L8-BO, binary PSCs were assembled following a conventional device configuration of indium tin oxide (ITO), ITO/PEDOT:PSS/PM6:acceptor/PNDIT-F3N/Ag. Detailed information on device fabrication and characterization can be found in the Supporting Information. The *J*–*V* curves of the blend films are shown in **Figure 3a**, and the corresponding photovoltaic parameters are summarized in **Table 1**. Figure 3b shows the PCE statistics of 20 cells for each D: A blend. Both the PM6:L8-BO and PM6: BTP-BO-4FO devices achieved efficiencies exceeding 17% without additives treatment. A slight enhancement was observed in the PM6:L8-BO (CN), achieving a PCE of 17.52%, featuring a V_{OC} of 0.879 V, a J_{SC} of 26.25 mA cm^{-2}, and an FF of 75.9%. In contrast, the PM6:L8-BO (DIO) based devices exhibited a notably improved performance, attaining a PCE of 18.2%, with a V_{OC} of 0.881 V, a J_{SC} of 26.50 mA cm^{-2}, and a significantly enhanced FF of 77.9%. This suggests that DIO serves as a superior additive for modulating film morphology in PM6:L8-BO systems.

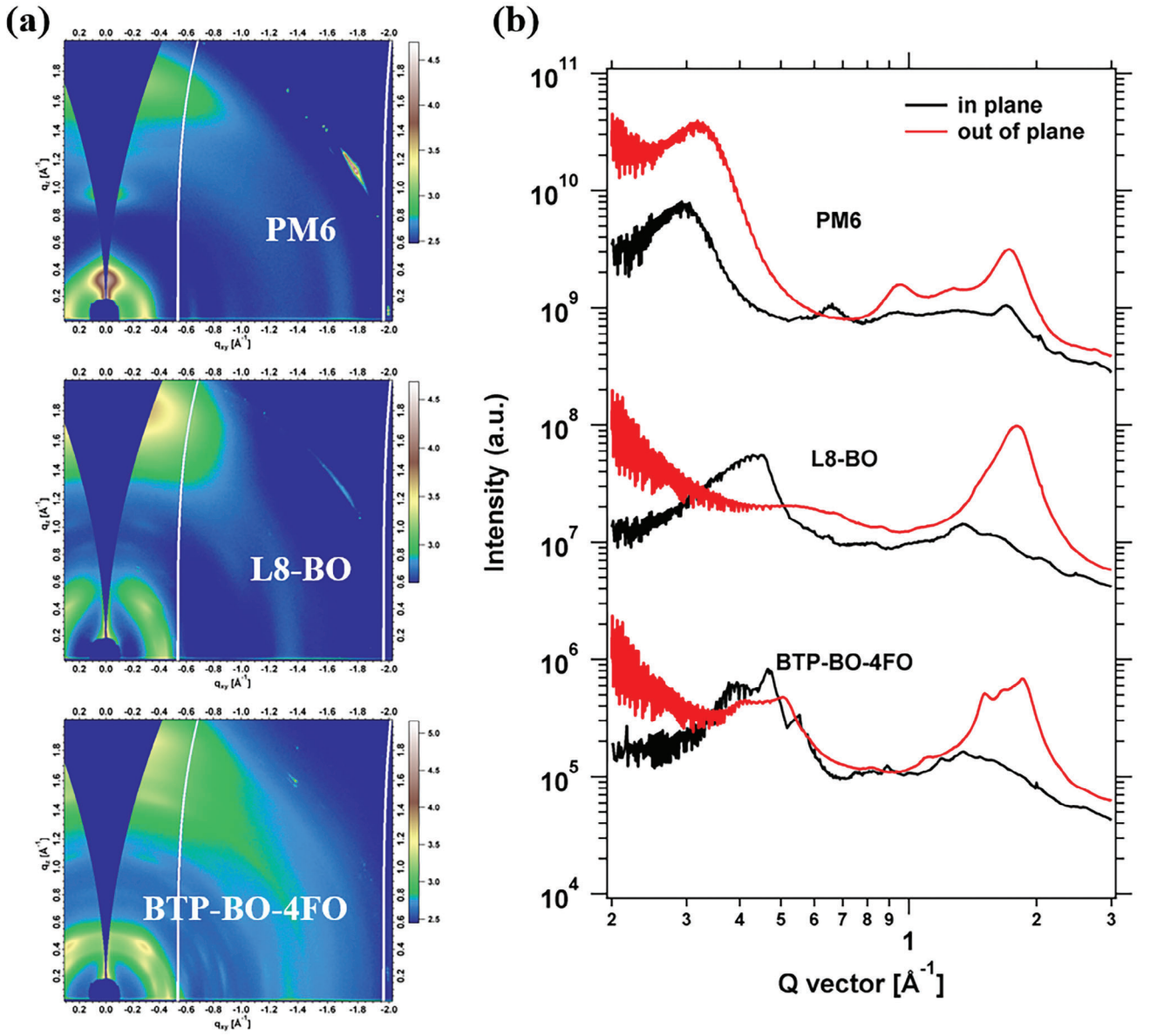

Figure 2. a) 2D-GIWAXS patterns of PM6, L8-BO, and BTP-BO-4FO neat films. b) Corresponding intensity profiles of PM6, L8-BO, and BTP-BO-4FO neat films along the in-plane (in black) and out-of-plane (in red) directions.

These results are consistent with the literature reports. However, for the PM6:BTP-BO-4FO blend, CN outperformed DIO, delivering a champion PCE of 18.62%, an outstanding V_{OC} of 0.933 V is obtained, accompanied by a J_{SC} of 25.79 mA cm^{-2}, and an FF of 77.4%. To the best of our knowledge, this represents the highest PCEs achieved for binary OPVs utilizing SMAs with asymmetric terminal groups, as shown in Figure 3c and Table S7 (Supporting Information).

The EQE measurements were conducted, and the results are presented in Figure 3d and Table 1. All kinds of OPVs achieved EQE values exceeding 80%. The PM6:L8-BO devices demonstrated broad and elevated EQE values spanning from 450–850 nm. The integrated J_{SC} values from the EQE curves are 25.21, 25.70, and 25.61 mA cm^{-2} for OPVs based on PM6:L8-BO, PM6:L8-BO (DIO), and PM6:L8-BO (CN), respectively, closely aligning with those derived from the *J*–*V* curves. While PM6:BTP-BTP-4FO devices exhibited a robust EQE response primarily within the 450–800 nm range. Notably, the EQE response between 650–800 nm of PM6: BTP-BO-4FO (CN) is even higher than PM6:L8-BO systems. The integrated J_{SC} values from the EQE curves are 24.37, 24.78, and 25.04 mA cm^{-2} for OPVs based on PM6:BTP-BO-4FO, PM6:BTP-BO-4FO (DIO) and PM6:BTP-BO-4FO (CN), respectively, consistent with the *J*sc values from the *J*–*V* curves with minimal deviations.

Device physics analyses are conducted alongside device efficiency measurements. The photocurrent versus effective voltage (J_{ph}-V_{eff}) curves are presented in Figure 3e, and the deduced saturated current density (J_{sat}), exciton dissociation, and collection

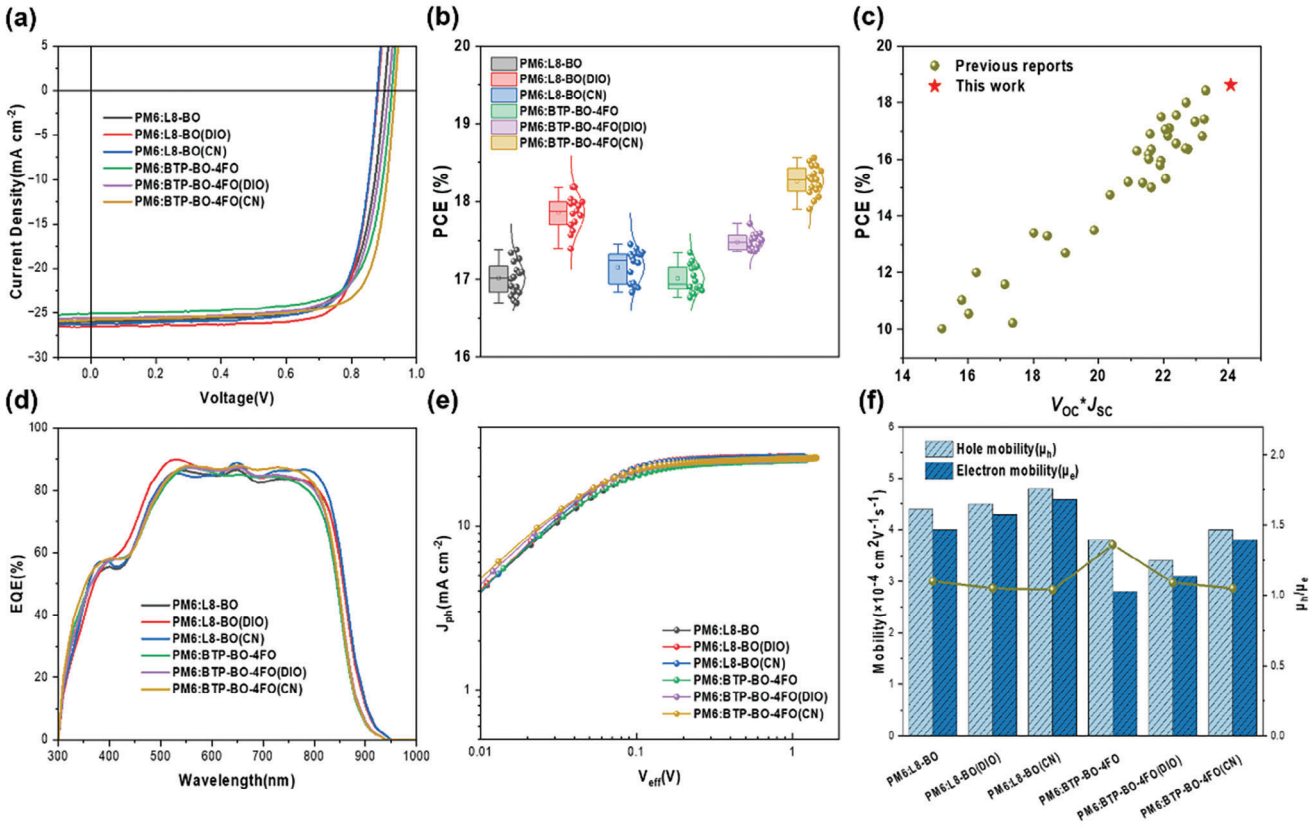

Figure 3. a) *J–V* curves of the blend films. b) Normal distribution of PCEs. c) A comparison of SMAs with asymmetric end groups. d) EQE curves of the blend films. e) J_{ph} versus V_{eff} of the blend films. f) Charge-carrier mobilities of the blend films.

efficiencies (η_{diss} & η_{coll}) are displayed in Table S2 (Supporting Information). Additives can enhance the saturated current density (J_{sat}) in both L8-BO and BTP-BO-4FO devices and a slight improvement in η_{diss} & η_{coll} was observed in PM6:L8-BO (DIO) devices and PM6:BTP-BO-4FO (CN) devices which is consistent with changes in J_{SC} and FF values. Also, another important factor correlated with FF is charge recombination. Consequently, light intensity dependent V_{OC} & J_{SC} curves are tested, illustrated in Figures S11 and S12 (Supporting Information), and further analyzed in Table S3 (Supporting Information). The outcomes exhibited a consistent trend with the changes in FF, particularly evident in the PM6:L8-BO (DIO) and PM6:BTP-BO-4FO (CN) blend films, showcasing reduced trap-assisted and bimolecular recombination. Besides, the carrier mobilities were measured by the space-charge-limited current (SCLC) method. The measurement results are shown in Figures S13 and S14 (Supporting Information), and the calculated electron/hole mobilities (μ_e/μ_h) can be found in Table S4 (Supporting Information) and illustrated in Figure 3f. From these results, we can know that the devices based on PM6:L8-BO (DIO) and PM6:BTP-BO-4FO (CN) presented higher and more balanced hole and electron mobilities, contributing to their superior J_{SC} and FF compared to the other devices.

Table 1. Photovoltaic parameters of the OPVs based on PM6:L8-BO and PM6: BTP-BO-4FO. The EQE-integrated current density values are put behind the slashes.

Active Layer	V_{OC} [V]	J_{SC} [mA cm^{-2}]	*FF* [%]	PCE [%]
PM6:L8-BO				
w/o	0.901	25.96/25.21	74.2	17.36
DIO	0.881	26.50/25.70	77.9	18.20
CN	0.879	26.25/25.61	75.9	17.52
PM6:BTP-BO-4FO				
w/o	0.924	25.05/24.37	74.8	17.33
DIO	0.913	25.55/24.78	75.4	17.59
CN	0.933	25.79/25.04	77.4	18.62

Then we turn on the focus to D/A blend films to further reveal the different morphology evolution caused by additive. GIWAXS measurements were utilized to explore the crystalline orderliness and molecular packing of the active layer. The 2D patterns and extracted line-cuts are presented in **Figure 4**. The *d*-spacing and crystalline coherence length (CCL) of molecular packing is also calculated and listed in Table S5 (Supporting Information). After blending with the donor PM6, the L8-BO blends demonstrate similar features with a lamellar peak at 0.31 Å^{-1} (d = 20.3 Å) in the IP direction and a strong π–π stacking peak at 1.78 Å^{-1} (d = 3.53 Å) in the OOP direction, consistent with the

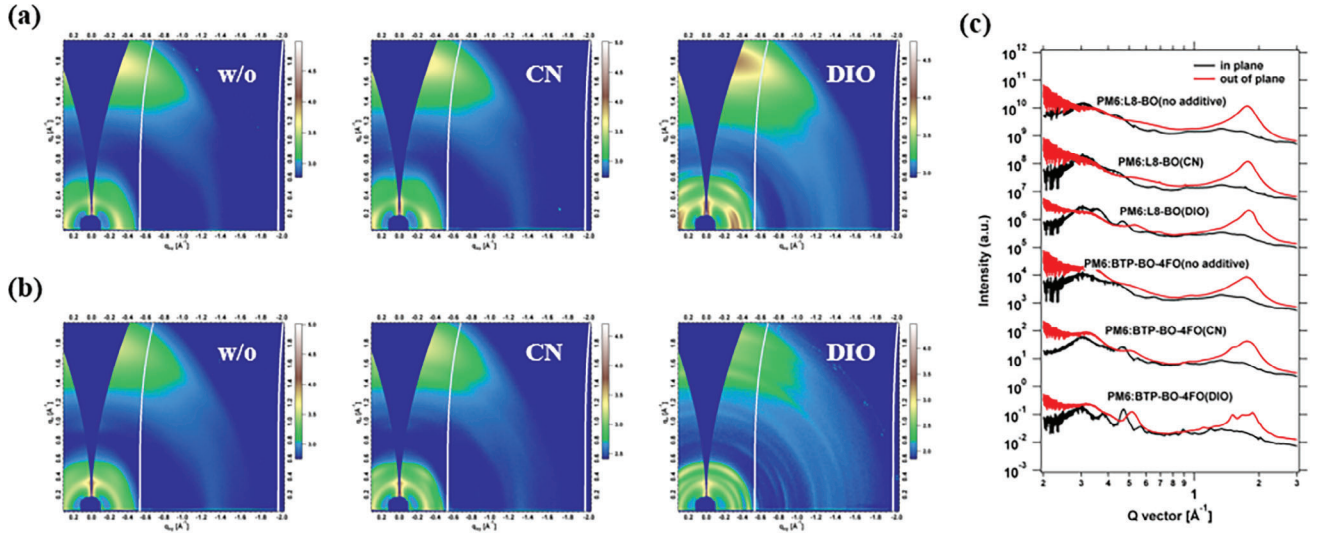

Figure 4. a) 2D GIWAXS images of the blend films. c) GIWAXS intensity profiles of the corresponding films along the in-plane (red lines) and out-of-plane (black lines) directions.

behavior observed in the neat films as discussed above. Among them, PM6:L8-BO (DIO) exhibited a more pronounced diffraction and a larger CCL (28.1 Å) in the out-of-plane (OOP) direction, suggesting enhanced crystalline ordering and stronger intermolecular interactions facilitated by DIO in the blend films, thereby leading to a higher *J*sc and FF of the corresponding devices. However, the alterations in crystalline order and molecular packing of PM6:BTP-BO-4FO (DIO) are excessive, from the CCL values (40.9 Å) and the d-spacing (3.35 Å) of the π–π stacking in the OOP direction, it can be inferred that DIO would cause over-aggregated BTP-BO-4FO agglomerates, thereby increasing the discrepancy in crystallinity between the acceptor and PM6, reflecting the scattering peaks still retained. In contrast, the PM6:BTP-BO-4FO (CN) blend could maintain the similar CCL (19.8 Å) of π–π stacking as that of neat acceptor while enhancing ordered crystalline of the lamellar packing in the IP direction with a CCL of 88.3 Å, similar to that PM6, which is conducive to the formation of interpenetrating network structures and improving the FF of devices, displaying a reduction in noise peaks in the IP and OOP orientations. This implies that CN treatment could refine the phase domain sizes to enhance the blending of donor and acceptor components without causing a pronounced shift in ordered/amorphous phase content, consequently benefiting both charge transfer and transport.

To analyze the surface topographies, atomic force microscopy (AFM) was initially employed. For an ideal blend morphology, continuous interpenetrating networks and nanoscale phase separations are essential.[43–45] The AFM images of blend films are displayed in Figure 4a, and the representative images of neat films are given in Figure S15 (Supporting Information), illustrating that these requirements were met for all blends, resulting in uniform surfaces with nanofiber-like features. Nonetheless, distinct morphology features were also observed. PM6:L8-BO (DIO) exhibited smaller domain sizes and a smoother surface, whereas PM6:L8-BO (CN) displayed larger and coarser fibers, potentially attributed to excessive phase separation. Equally, the PM6:BTP-BO-4FO (CN) demonstrated an intermediate morphology between PM6: BTP-BO-4FO and PM6:BTP-BO-4FO (DIO), manifesting more favorable phase separation behavior. This suggests that the asymmetric terminal group in BTP-BO-4FO could influence the phase separation behavior.

Figure 5b,c presents the photoluminescence (PL) spectra of the acceptors L8-BO and BTP-BO-4FO, along with different blend films. Compared to their pristine films, all blend films displayed high PL quenching efficiencies and significantly reduced PL intensities. PM6:L8-BO-based devices demonstrated comparable PL quenching efficiency, exceeding 90% in all blend films due to the effective blending of donor and acceptor components. While the PL quenching efficiency of DIO (86.5%) was notably lower than that of CN (93.6%) and no additive (93.4%) in the PM6:BTP-BO-4FO systems, revealing that the film treated by CN could provide sufficient D/A interfaces for charge transfer from PM6 to BTP-BO-4FO, correlated with its better performance of the device.

Finally, the charge behavior is investigated by the femtosecond transient absorption spectroscopy (fs-TAS) technology, as an important supplementary study aside from the morphology analysis.[46–48] The polarons generation kinetics were fitted using the sum of exponentials. In all cases herein, the bi-exponential function can describe the polarons generation dynamics. The fast component can be attributed to the dissociation of the photogenerated acceptor singlet excitons formed within the vicinity of D:A interfaces. Meanwhile, the slow component can be attributed to the diffusion-limited process of singlet excitons formed within pure domains. The TAS representative spectra of acceptor-only and blend films and their pseudo-2D color maps are all shown in **Figures 6** and S16 (Supporting Information), and correlated data are further analyzed in Table S6 (Supporting Information). For PM6:L8-BO systems, based on the slow component, it can be observed that CN causes a slight kinetics (9.43 ps) while a substantially slower process is observed for DIO (12.33 ps). Meanwhile, the fast component displays the same trend. It has

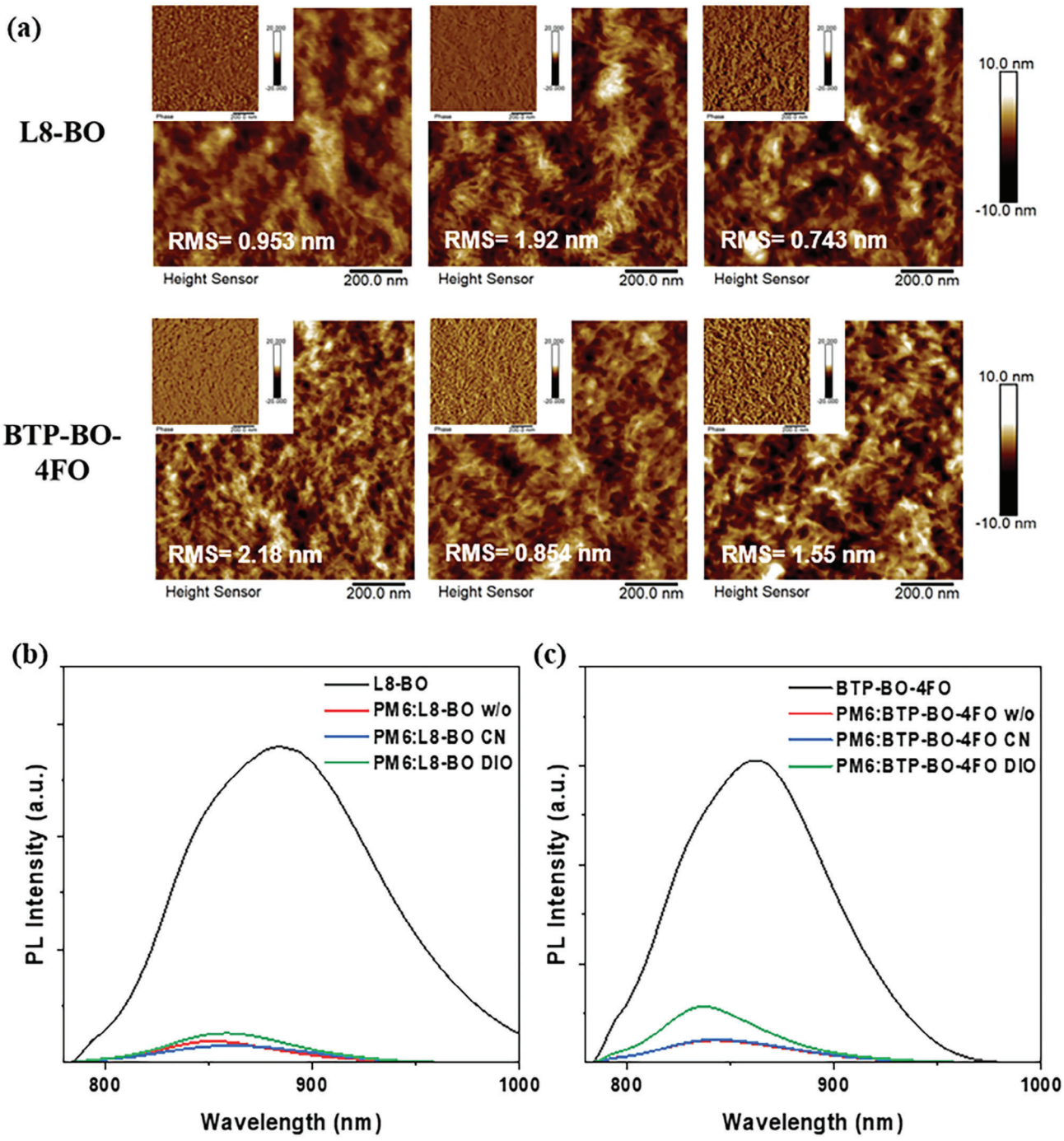

Figure 5. a) AFM height images and phase images (upper left corner) of blend films. From left to right is no additive, CN, DIO. b) PL spectra of L8-BO and the blend films. c) PL spectra of BTP-BO-4FO and the blend films.

already been reported that the bulk-to-interface energy landscape can contribute to a slow yet still efficient excitons dissociation process can exist.[49–50] In fact, a slow singlet exciton dissociation process caused by the interface energy cascade is previously shown to possibly enhance the dissociation of the singlet excitons at the donor–acceptor interface regime. Hence, the slower processes observed herein should not be attributed to geminate recombination. Instead, it can be argued to also assist the dissociation of the singlet excitons, as can be inferred from the improved J_{SC}. For PM6:BTP-BO-4FO systems, the impact of CN in the kinetics is marginal and similar with the blends without additive treatments (i.e., considering both the fast and slow components). On the other hand, the sample treated with DIO shows a much faster process for the fast component (< 0.2 ps) while

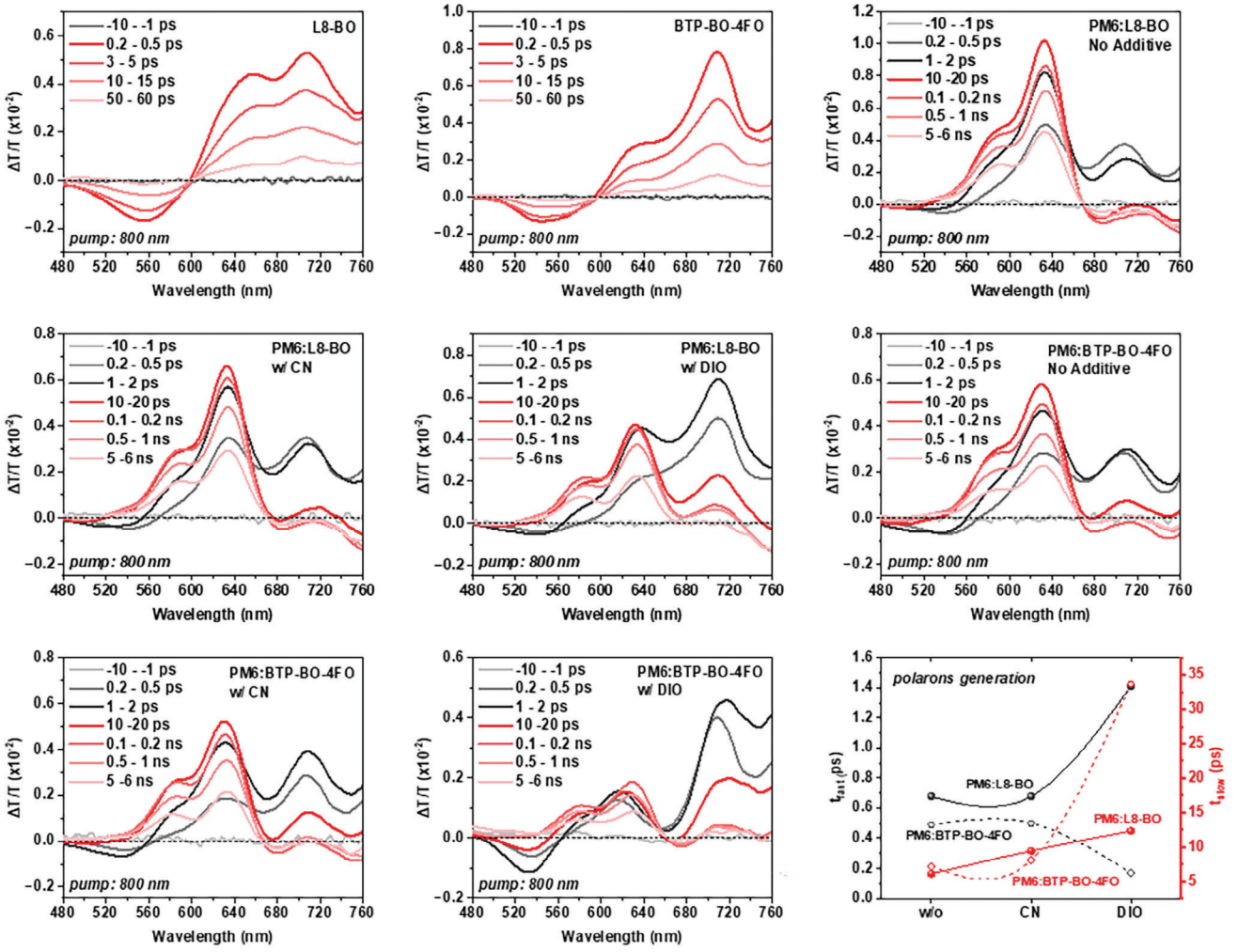

Figure 6. Transient absorption spectral line cuts and the corresponding polarons generation rate after selective acceptor excitation using 800 nm pump laser of fluence 3 uJ cm^{-2}. The polarons generation rates are based on acceptor hole transfer to the donor, fitted using a sum of exponentials with fast and slow components.

the slow component is prolonged similar with the PM6:L8-BO binary. These suggests that the PM6:BTP-BO-4FO (DIO) reduced the intermixing phase. Overall, we didn't observe a significant increase in J_{SC} for PM6:BTP-BO-4FO (DIO) devices which could be due to a trade-off effect caused by intermixing phase reduction.

As shown in Figure S17 (Supporting Information), the polarons of blend films are detected at 570–585 nm and assessed to characterize the sub-nanosecond scale recombination kinetics. For all the samples, the sub-ns polarons recombination appears slightly slower than w/o additives. This is known to reduce the bimolecular free charge recombination which can benefit the free charge transport and thereby the device FF.[51–53] But the overall device FF will reflect the overall recombination property (i.e., the combination of both bimolecular and monomolecular losses). Besides, these parameters are significantly influenced by the intricate interplay of nanomorphology and molecular packing, which governs the diffusion of singlet excitons and the long-range transport of polarons above a few ns. Therefore, the charge dynamic study should combine with morphology data to jointly analyze device performance.

3. Conclusion

In conclusion, through the development of a unique difluorine- and methoxy-co-substituted terminal group and the application of an asymmetric substitution approach, a novel small molecule acceptor named BTP-BO-4FO is synthesized. CV measurements, DFT calculations, and GIWAXS display elevated energy levels and enhanced crystallinity in comparison to the symmetric counterpart of L8-BO. When combined with PM6, the resulting OPVs demonstrated satisfactory PCE exceeding 17% without additives, showcasing comparable performance to L8-BO but with notable advantages in V_{OC}. Furthermore, the PM6:BTP-BO-4FO presented distinct parameter variations in devices treated with two common additives CN and DIO, morphological analyses and photophysical characterizations were carried out to unveil the reasons. The BTP-BO-4FO blend films treated with CN

can not only diminish the variation in the size of the intermixed phase but also maintain appropriate pure domain sizes, thereby enhancing exciton dissociation and charge transport to boost the J_{SC} and FF of the device, culminating in an impressive PCE of 18.62%. Overall, this work demonstrates that asymmetric terminal design is a feasible strategy to improve charge separation and fine-tune energy levels simultaneously for high-performance OPVs, paving the way for pursuing carbon neutrality.[38,54–55]

Supporting Information

Supporting Information is available from the Wiley Online Library or from the author.

Acknowledgements

R. M. thanks for the support from PolyU Distinguished Postdoc Fellowship (1-YW4C). Z.L. thanks the National Natural Science Foundation of China (NSFC, No. 22309119). H.Y. appreciates the support from the National Key Research and Development Program of China (No. 2019YFA0705900) funded by MOST, the Basic and Applied Research Major Program of Guangdong Province (No. 2019B030302007), National Natural Science Foundation of China (NSFC, No. 22075057), the Shen Zhen Technology and Innovation Commission through (Shenzhen Fundamental Research Program, JCYJ20200109140801751), the Hong Kong Research Grants Council (research fellow scheme RFS2021-6S05, RIF project R6021-18, CRF project C6023-19G, GRF project 16310019, 16310020, 16309221, and 16309822), Hong Kong Innovation and Technology Commission (ITC-CNERC14SC01), Foshan-HKUST (Project NO. FSUST19-CAT0202), Zhongshan Municipal Bureau of Science and Technology (No. ZSST20SC02), Guangdong-Hong Kong-Macao Joint Laboratory (No.2023B1212120003) and Tencent Xplorer Prize. J.W. thanks the Guangdong government and the Guangzhou government for funding (2021QN02C110), the Guangzhou Municipal Science and Technology Project (No. 2023A03J0097 and No. 2023A03J0003), and NSFC (52303249). G.L. thanks the support from Research Grants Council of Hong Kong (Project Nos 15221320, 15307922, C5037-18G, C4005-22Y), RGC Senior Research Fellowship Scheme (SRFS2223-5S01), the Hong Kong Polytechnic University: Sir Sze-yuen Chung Endowed Professorship Fund (8-8480), RISE (Q-CDBK), PRI (Q-CD7X), G-SAC5 and Guangdong-Hong Kong-Macao Joint Laboratory for Photonic-Thermal-Electrical Energy Materials and Devices (GDSTC No. 2019B121205001). This research used resources from the Advanced Light Source, which is a DOE Office of Science User Facility under contract no. DE-AC02-05CH11231.

Conflict of Interest

The authors declare no conflict of interest.

Author Contributions

W.W. and B.Z. contributed equally to this work. W.W. and B.Z. performed investigation, formal analysis, conceptualization, and wrote the original draft; R.M. performed project administration, supervision, conceptualization, acquired resources, and wrote, reviewed and edited the final manuscript; J.Y., C.L., B.X., and M.Q. performed investigation; Z.L. performed supervision, methodology, and wrote, reviewed and edited the final manuscript; T.A.D.P. performed investigation, formal analysis; M.L., J.W., Q.F., W.M., C.Y., and G.L. acquired resources; H.Y. acquired resources and performed supervision.

Data Availability Statement

The data that support the findings of this study are available from the corresponding author upon reasonable request.

Keywords

asymmetric acceptor, difluoro-methoxylated end-group, organic photovoltaic, power conversion efficiency

Received: April 8, 2024
Revised: April 28, 2024
Published online: May 16, 2024

[1] Y. Liu, B. Liu, C.-Q. Ma, F. Huang, G. Feng, H. Chen, J. Hou, L. Yan, Q. Wei, Q. Luo, Q. Bao, W. Ma, W. Liu, W. Li, X. Wan, X. Hu, Y. Han, Y. Li, Y. Zhou, Y. Zou, Y. Chen, Y. Li, Y. Chen, Z. Tang, Z. Hu, Z.-G. Zhang, Z. Bo, *Sci China Chem* **2022**, *65*, 224.
[2] Y. Liu, B. Liu, C.-Q. Ma, F. Huang, G. Feng, H. Chen, J. Hou, L. Yan, Q. Wei, Q. Luo, Q. Bao, W. Ma, W. Liu, W. Li, X. Wan, X. Hu, Y. Han, Y. Li, Y. Zhou, Y. Zou, Y. Chen, Y. Liu, L. Meng, Y. Li, Y. Chen, Z. Tang, Z. Hu, Z.-G. Zhang, Z. Bo, *Sci China Chem* **2022**, *65*, 1457.
[3] K. Liu, Y. Jiang, G. Ran, F. Liu, W. Zhang, X. Zhu, *Joule* **2024**, *8*, 835.
[4] C. Wang, X. Ma, Y.-f. Shen, D. Deng, H. Zhang, T. Wang, J. Zhang, J. Li, R. Wang, L. Zhang, Q. Cheng, Z. Zhang, H. Zhou, C. Tian, Z. Wei, *Joule* **2023**, *7*, 2386.
[5] H. Hu, S. Liu, J. Xu, R. Ma, Z. Peng, T. A. D. Peña, Y. Cui, W. Liang, X. Zhou, S. Luo, H. Yu, M. Li, J. Wu, S. Chen, G. Li, Y. Chen, *Angew. Chem., Int. Ed.* **2024**, *63*, e202400086.
[6] X. Xu, W. Jing, H. Meng, Y. Guo, L. Yu, R. Li, Q. Peng, *Adv. Mater.* **2023**, *35*, 2208997.
[7] R. Ma, X. Jiang, J. Fu, T. Zhu, C. Yan, K. Wu, P. Müller-Buschbaum, G. Li, *Energy Environ. Sci.* **2023**, *16*, 2316.
[8] Z. Gan, L. Wang, J. Cai, C. Guo, C. Chen, D. Li, Y. Fu, B. Zhou, Y. Sun, C. Liu, J. Zhou, D. Liu, W. Li, T. Wang, *Nat. Commun.* **2023**, *14*, 6297.
[9] J. Wang, Y. Wang, P. Bi, Z. Chen, J. Qiao, J. Li, W. Wang, Z. Zheng, S. Zhang, X. Hao, J. Hou, *Adv. Mater.* **2023**, *35*, 2301583.
[10] W. Wu, Y. Luo, T. A. Dela Peña, J. Yao, M. Qammar, M. Li, H. Yan, J. Wu, R. Ma, G. Li, *Adv. Energy Mater.* **2024**, *14*, 2400354.
[11] S. Chen, S. Zhu, L. Hong, W. Deng, Y. Zhang, Y. Fu, Z. Zhong, M. Dong, C. Liu, X. Lu, K. Zhang, F. Huang, *Angew. Chem., Int. Ed.* **2024**, *63*, e202318756.
[12] X. Liu, Z. Zhang, C. Wang, C. Zhang, S. Liang, H. Fang, B. Wang, Z. Tang, C. Xiao, W. Li, *Angew. Chem., Int. Ed.* **2024**, *63*, e202316039.
[13] X. Li, A. Tang, H. Wang, Z. Wang, M. Du, Q. Guo, Q. Guo, E. Zhou, *Angew. Chem., Int. Ed.* **2023**, *62*, e202306847.
[14] X. Kong, L. Zhan, S. Li, S. Yin, H. Qiu, Y. Fu, X. Lu, Z. Chen, H. Zhu, W. Fu, H. Chen, *Chem. Eng. J.* **2023**, *473*, 145201.
[15] Z. Zheng, J. Wang, P. Bi, J. Ren, Y. Wang, Y. Yang, X. Liu, S. Zhang, J. Hou, *Joule* **2022**, *6*, 171.
[16] L. Zhu, M. Zhang, W. Zhong, S. Leng, G. Zhou, Y. Zou, X. Su, H. Ding, P. Gu, F. Liu, Y. Zhang, *Energy Environ. Sci.* **2021**, *14*, 4341.
[17] W. Ma, C. Yang, X. Gong, K. Lee, A. J. Heeger, *Adv. Funct. Mater.* **2005**, *15*, 1617.
[18] R. Ma, H. Li, T. A. Dela Peña, X. Xie, P. W.-K. Fong, Q. Wei, C. Yan, J. Wu, P. Cheng, M. Li, G. Li, *Adv. Mater.* **2024**, *36*, 2304632.
[19] H. Lai, H. Chen, Z.-Y. Chen, Y. Lang, Y. Zhu, S.-T. Zhang, X. Lai, P. Tan, Y. Zhang, B. Yang, G. Li, F. He, *Energy Environ. Sci.* **2023**, *16*, 5944.
[20] J. Shi, Z. Chen, H. Liu, Y. Qiu, S. Yang, W. Song, Z. Ge, *Adv. Energy Mater.* **2023**, *13*, 2301292.
[21] M. Yang, X. Tan, B. Yin, S. Kim, S. Pang, Z. Chen, X. Yang, C. Yang, Z. Liu, C. Duan, *ACS Energy Lett.* **2023**, *8*, 2641.
[22] W. Wei, C. e. Zhang, Z. Chen, W. Chen, G. Ran, G. Pan, W. Zhang, P. Müller-Buschbaum, Z. Bo, C. Yang, Z. Luo, *Angew. Chem., Int. Ed.* **2024**, *63*, e202315625.
[23] C. Yang, S. Zhang, J. Ren, M. Gao, P. Bi, L. Ye, J. Hou, *Energy Environ. Sci.* **2020**, *13*, 2864.

[24] J. Ge, L. Hong, H. Ma, Q. Ye, Y. Chen, L. Xie, W. Song, D. Li, Z. Chen, K. Yu, J. Zhang, Z. Wei, F. Huang, Z. Ge, *Adv. Mater.* **2022**, *34*, 2202752.
[25] D. Li, C. Sun, T. Yan, J. Yuan, Y. Zou, *ACS Cent. Sci.* **2021**, *7*, 1787.
[26] J. Guo, X. Xia, B. Qiu, J. Zhang, S. Qin, X. Li, W. Lai, X. Lu, L. Meng, Z. Zhang, Y. Li, *Adv. Mater.* **2023**, *35*, 2211296.
[27] X. Zhao, Q. An, H. Zhang, C. Yang, A. Mahmood, M. Jiang, M. H. Jee, B. Fu, S. Tian, H. Y. Woo, Y. Wang, J.-L. Wang, *Angew. Chem., Int. Ed.* **2023**, *62*, e202216340.
[28] Y. Gao, X. Yang, W. Wang, R. Sun, J. Cui, Y. Fu, K. Li, M. Zhang, C. Liu, H. Zhu, X. Lu, J. Min, *Adv. Mater.* **2023**, *35*, 2300531.
[29] C. He, Q. Shen, B. Wu, Y. Gao, S. Li, J. Min, W. Ma, L. Zuo, H. Chen, *Adv. Energy Mater.* **2023**, *13*, 2204154.
[30] Q. Fan, R. Ma, J. Yang, J. Gao, H. Bai, W. Su, Z. Liang, Y. Wu, L. Tang, Y. Li, Q. Wu, K. Wang, L. Yan, R. Zhang, F. Gao, G. Li, W. Ma, *Angew. Chem., Int. Ed.* **2023**, *62*, e202308307.
[31] Y. Zhang, Y. Ji, Y. Zhang, W. Zhang, H. Bai, M. Du, H. Wu, Q. Guo, E. Zhou, *Adv. Funct. Mater.* **2022**, *32*, 2205115.
[32] T. Dai, A. Tang, Y. Meng, C. Dong, P. Cong, J. Lu, J. Du, Y. Zhong, E. Zhou, *Angew. Chem., Int. Ed.* **2024**, e202403051.
[33] C. He, Z. Chen, T. Wang, Z. Shen, Y. Li, J. Zhou, J. Yu, H. Fang, Y. Li, S. Li, X. Lu, W. Ma, F. Gao, Z. Xie, V. Coropceanu, H. Zhu, J.-L. Bredas, L. Zuo, H. Chen, *Nat. Commun.* **2022**, *13*, 2598.
[34] Y. Cui, P. Zhu, H. Hu, X. Xia, X. Lu, S. Yu, H. Tempeld, R.-A. Eichel, X. Liao, Y. Chen, *Angew. Chem., Int. Ed.* **2023**, *62*, e202304931.
[35] B. Zou, W. Wu, T. A. Dela Peña, R. Ma, Y. Luo, Y. Hai, X. Xie, M. Li, Z. Luo, J. Wu, C. Yang, G. Li, H. Yan, *Nano-Micro Lett.* **2023**, *16*, 30.
[36] T. Lu, F. Chen, *J. Comput. Chem.* **2012**, *33*, 580.
[37] T. Xu, Z. Luo, R. Ma, Z. Chen, T. A. Dela Peña, H. Liu, Q. Wei, M. Li, C. e. Zhang, J. Wu, X. Lu, G. Li, C. Yang, *Angew. Chem., Int. Ed.* **2023**, *62*, e202304127.
[38] W. Gao, R. Ma, T. A. Dela Peña, C. Yan, H. Li, M. Li, J. Wu, P. Cheng, C. Zhong, Z. Wei, A. K. Y. Jen, G. Li, *Nat. Commun.* **2024**, *15*, 1946.
[39] P. Müller-Buschbaum, *Adv. Mater.* **2014**, *26*, 7692.
[40] J. Rivnay, S. C. B. Mannsfeld, C. E. Miller, A. Salleo, M. F. Toney, *Chem. Rev.* **2012**, *112*, 5488.
[41] W. Wei, R. Ma, Z. Chen, T. Xu, G. Li, Z. Luo, *Chin. J. Chem.* **2024**, *42*, 623.
[42] H. Bai, R. Ma, W. Su, T. A. D. Peña, T. Li, L. Tang, J. Yang, B. Hu, Y. Wang, Z. Bi, Y. Su, Q. Wei, Q. Wu, Y. Duan, Y. Li, J. Wu, Z. Ding, X. Liao, Y. Huang, C. Gao, G. Lu, M. Li, W. Zhu, G. Li, Q. Fan, W. Ma, *Nano-Micro Lett.* **2023**, *15*, 241.
[43] D. Li, N. Deng, Y. Fu, C. Guo, B. Zhou, L. Wang, J. Zhou, D. Liu, W. Li, K. Wang, Y. Sun, T. Wang, *Adv. Mater.* **2023**, *35*, 2208211.
[44] B. Liu, W. Xu, R. Ma, J.-W. Lee, T. A. Dela Peña, W. Yang, B. Li, M. Li, J. Wu, Y. Wang, C. Zhang, J. Yang, J. Wang, S. Ning, Z. Wang, J. Li, H. Wang, G. Li, B. J. Kim, L. Niu, X. Guo, H. Sun, *Adv. Mater.* **2023**, *35*, 2308334.
[45] L. Ye, Y. Yang, C. Liu, X. Duan, S. Wang, W. Li, X. Sun, T. Wang, W. Ma, W. Li, Y. Sun, *Small* **2023**, *19*, 2303226.
[46] Y. Tamai, Y. Murata, S.-i. Natsuda, Y. Sakamoto, *Adv. Energy Mater.* **2024**, *14*, 2301890.
[47] D. Jiang, J. Sun, R. Ma, V. K. Wong, J. Yuan, K. Gao, F. Chen, S. K. So, X. Hao, G. Li, H. Yin, *Mater. Sci. and Eng.: R* **2024**, *157*, 100772.
[48] Z. Chen, C. He, P. Ran, X. Chen, Y. Zhang, C. Zhang, R. Lai, Y. Yang, H. Chen, H. Zhu, *Energy Environ. Sci.* **2023**, *16*, 3373.
[49] S. Natsuda, T. Saito, R. Shirouchi, Y. Sakamoto, T. Takeyama, Y. Tamai, H. Ohkita, *Energy Environ. Sci.* **2022**, *15*, 1545.
[50] T. A. Dela Peña, R. Ma, Z. Xing, Q. Wei, J. I. Khan, R. M. Young, Y. Hai, S. A. Garcia, X. Zou, Z. Jin, F. L. Ng, K. L. Yeung, D. F. Swearer, M. R. Wasielewski, J. Wang, H. Cha, H. Yan, K. S. Wong, G. Li, M. Li, J. Wu, *Energy Environ. Sci.* **2023**, *16*, 3416.
[51] W. Liang, L. Chen, Z. Wang, Z. Peng, L. Zhu, C. H. Kwok, H. Yu, W. Xiong, T. Li, Z. Zhang, Y. Wang, Y. Liao, G. Zhang, H. Hu, Y. Chen, *Adv. Energy Mater.* **2024**, *14*, 2303661.
[52] L. Chen, J. Yi, R. Ma, T. A. Dela Peña, Y. Luo, Y. Wang, Y. Wu, Z. Zhang, H. Hu, M. Li, J. Wu, G. Zhang, H. Yan, G. Li, *Mater. Sci. Eng.: R* **2024**, *159*, 100794.
[53] L. Chen, R. Ma, J. Yi, T. A. Dela Peña, H. Li, Q. Wei, C. Yan, J. Wu, M. Li, P. Cheng, H. Yan, G. Zhang, G. Li, *Aggregate* **2024**, *5*, e455.
[54] H. Zhu, Y. Li, *Green Carbon* **2023**, *1*, 14.
[55] R. Ma, Q. Fan, T. A. Dela Peña, B. Wu, H. Liu, Q. Wu, Q. Wei, J. Wu, X. Lu, M. Li, W. Ma, G. Li, *Adv. Mater.* **2023**, *35*, 2212275.